

swordfish: Efficient Forecasting of New Physics Searches without Monte Carlo

Thomas D. P. Edwards^{1,*} and Christoph Weniger^{1,†}

¹*Gravitation Astroparticle Physics Amsterdam (GRAPPA),
Institute for Theoretical Physics Amsterdam and Delta Institute for Theoretical Physics,
University of Amsterdam, Science Park 904, 1090 GL Amsterdam, The Netherlands*

(Dated: Compiled on February 18, 2022)

We introduce **swordfish**,^a a Monte-Carlo-free Python package to predict expected exclusion limits, the discovery reach and expected confidence contours for a large class of experiments relevant for particle- and astrophysics. The tool is applicable to any counting experiment, supports general correlated background uncertainties, and gives exact results in both the signal- and systematics-limited regimes. Instead of time-intensive Monte Carlo simulations and likelihood maximization, it internally utilizes new approximation methods that are built on information geometry. Out of the box, **swordfish** provides straightforward methods for accurately deriving many of the common sensitivity measures. In addition, it allows one to examine experimental abilities in great detail by employing the notion of *information flux*. This new concept generalizes signal-to-noise ratios to situations where background uncertainties and component mixing cannot be neglected. The user interface of **swordfish** is designed with ease-of-use in mind, which we demonstrate by providing typical examples from indirect and direct dark matter searches as **jupyter notebooks**.

I. INTRODUCTION

Sensitivity to signs of new physics is the most desirable feature of a future experiment. As such, optimizing the process by which these sensitivities are calculated is of utmost importance for efficient scientific progress. Calculating the projected sensitivity of various experiments has proven, in the past, to be a computationally expensive task. From experimentalists looking to optimize the parameter space they rule out to theorists calculating whether their particle physics model will be observable in the future, sensitivity projections are a ubiquitous task among physicists and astronomers.

The most commonly used sensitivity calculations are based on the maximum likelihood ratio (MLR) method which, in the large-sample (Gaussian) limit, behaves in a well defined way [1]. The Fisher Information matrix is connected, through the Cramer-Rao bound [2], to the full covariance of the model parameters without the need for computationally expensive Monte Carlo (MC) simulations. This becomes even more important in the small-sample (Poisson) limit when asymptotic distributions of the MLR break down. In the past the Poisson limit is the precise regime in which the Fisher method also breaks down.

Ref. [3] presents the *equivalent counts* (EC) method which extends the Fisher formalism to the Poisson regime by condensing the complexity of calculating exclusion limits and the discovery reach into just two numbers, equivalent signal and background counts. The success of this method comes from the mapping between profiled log-likelihood ratios and the log-Poisson ratio explained in Sec. II. Most importantly the EC method is

designed to be accurate in both the Poisson and Gaussian regimes, making it a very powerful forecasting tool for a large variety of counting experiments. In addition to its high accuracy it remains fast and simple to calculate even when encountering many parameters in the Poisson regime, which has traditionally been extremely time consuming due to the large number of MCs required to accurately map the MLR.

swordfish is a complete and rigorous python package to efficiently manage and perform all calculations proposed in Ref. [3] in addition to some new techniques we introduce here. We provide here a comprehensive review of the capabilities of **swordfish** to calculate the main quantities of interest, namely exclusion limits and the discovery reach. We also emphasize a concept we named the *information flux* which acts as a generalization of signal-to-noise ratio (SNR) by taking into account arbitrary systematics between background components.

Traditionally the Fisher information matrix is visualized by viewing its eigenvalues and eigenvectors as the magnitude and directions of the axes of an ellipse. Unfortunately this does not capture the full shape of the parameter space. A major benefit of the Fisher Information matrix is that it can be treated as a metric on the space of model parameters, allowing for unique visualization schemes which have been developed in the field of *information geometry*. We present two main examples: The first is designed to match as closely as possible the traditional confidence contours used for parameter reconstruction. We use the geodesic equation as defined by the Fisher metric to trace the local curvature of the parameter space which is then easily relatable to a distance scale in terms of standard deviations and allows for the construction of a non-ellipsoidal contour. The second is a more generalized visualization scheme using streamlines which represent approximate 1σ boxes in the parameter space. When lines become too far apart an additional line is added to maintain the 1σ separation. Both of

* t.d.p.edwards@uva.nl

† c.weniger@uva.nl

^a github.com/cweniger/swordfish

these schemes are fully contained within **swordfish** and are therefore easy and fast to produce.

A typical problem for both experimental and theoretical physicists is calculating whether models are discriminable by future experiments. In high dimensional parameter this is best done by comparison pair-wise comparison of more than 100 million parameter points. To that end we introduce the *Euclideanized signal* method which approximately maps the a signal to a new vector which can then be used to calculate the Euclidean distance between points. This mapping allows for extremely efficient comparison of a large number of points using modern clustering algorithms but only work in Euclidean space.

Indirect and direct dark matter (DM) searches are set to make significant gains over the next few years with the construction of multiple new experiments. We here confirm the results EC method by producing approximate DM sensitivity forecasts for a couple of well known future/current generation experiments, namely the Cherekov Telescope array (CTA) and Xenon 1T.

This paper is structured as follows. In Sec. II we present the interface to **swordfish** and provide descriptions of all the concepts required to understand the EC method¹. Sec. III implements **swordfish** projected exclusion limits for both indirect and direct DM searches before discussing the novel visualizations of the parameter space. In Sec. IV we conclude. Additional mathematical details and verification of the methods can be found in the Appendix.

II. STRUCTURE OF PACKAGE

We here give a basic overview of the package with accompanying descriptions of the various statistical techniques and approximations used. For more mathematical details see A as well as Ref. [3].

A. Model definition

The log-likelihood function of the model that is implemented in **swordfish** is a general Poisson likelihood,

$$\ln \mathcal{L}_p(\mathcal{D}|\mathbf{S}) = \max_{\delta\mathbf{B}} \left(\underbrace{\sum_{i=1}^{n_b} (d_i \cdot \ln \mu_i(\mathbf{S}, \delta\mathbf{B}) - \mu_i(\mathbf{S}, \delta\mathbf{B}))}_{(1)} - \underbrace{\frac{1}{2} \sum_{i,j=1}^{n_b} \delta B_i (K^{-1})_{ij} \delta B_j}_{(4)} \right). \quad (1)$$

Here, the expectation values μ_i for the number of events in bins $i = 1, \dots, n_b$ are given by a sum of the signal S_i and background B_i , as well as background perturbations δB_i , multiplied by the exposure E_i :

$$\mu_i(\mathbf{S}, \delta\mathbf{B}) = \left(\underbrace{S_i}_{(2)} + \underbrace{B_i}_{(4)} + \underbrace{\delta B_i}_{(3)} \right) \cdot \underbrace{E_i}_{(3)}. \quad (2)$$

The matrix K describes the covariance of the background perturbations δB_i . Background perturbations are limited to Gaussian variations but otherwise completely flexible. Since the background perturbations are usually not of interest, they are always implicitly profiled out as indicated in the definition of \mathcal{L}_p , Eq. (1).

The individual terms of the profile likelihood and the expectation values have the following meaning.

- (1) Conventional Poisson log-likelihood (up to a constant term that does only depend on data and not affect Frequentist inference).

- (2) Linear model, defined through one fixed ('background' or 'base') component \mathbf{B} , the background perturbations $\delta\mathbf{B}$, and a signal component $\mathbf{S}^{(k)}$. The latter can be often a function of model parameters θ (a parametric background model is instead split up in a base part \mathbf{B} and its variations K).

- (3) Exposure. It is defined such that μ_i is dimensionless and corresponds to expected counts in bin i . The physical units of the exposure and the signal and background components is up to the user and situation dependent. Factoring out exposure in the definitions is necessary for the definition of *information flux* further below.

- (4) Correlated background perturbations with a covariance matrix K_{ij} of size $n_b \times n_b$. If the number of bins is large, this introduces an equally large number of additional nuisance parameters in the problem. Our approach handles these efficiently.

A few final remarks about the model in Eq. (1) are in order. The expectation values μ_i as defined in Eq. (2) are not automatically positive. For large enough variances K , the δB_i can become negative enough to change

¹ For more mathematical details see Ref. [3]

the sign of μ_i . The physical constraint $B_i + \delta B_i \geq 0$ cannot be directly implemented in our treatment. A straightforward solution to this problem would be to replace $B_i + \delta B_i \mapsto B_i \exp(\delta B_i/B_i)$. If we were to do a similar transformation for the signal model, the resulting model for μ_i would be positive for any model parameters. Such a scenario, a mixture between a Poisson process and a Gaussian random field, is known as Cox process [4]. However, although this model has more appealing mathematical properties, it somehow dilutes the connection with the typical (usually additive) models one encounters in particle and astro-particle physics. Furthermore, up to the second derivative of the model parameters, which is what we are interested in here, both models would give identical analytic results.

B. Overview

In Fig. 1, we provide a conceptual summary of the calculations that can be performed with `swordfish` and their relations. Our ‘counting experiment’ is fully defined by the (potentially parametric) signal $\mathbf{S}(\boldsymbol{\theta})$, the base background \mathbf{B} and its perturbations δB as described by the covariance matrix K , and the exposure \mathbf{E} . Based on this model, the Fisher information matrix can be calculated. The Fisher matrix can then be used in various ways. First, for fixed signal shapes with a free normalization, it is possible to use the equivalent counts method to forecast exclusion limits and the discovery reach of the implemented counting experiment. Second, one generates a field of Fisher information matrices, which gives rise to a metric in the space of model parameters. This metric can be used to derive expected confidence contours for parameter reconstruction, or it can be visualized directly using adaptive density streamlines. Thirdly, the Euclideanized signal method can be used to calculate the discrimination power of the counting experiment w.r.t. various signal benchmark models. This ansatz can again be used to derive confidence contours. Lastly, it is possible to calculate the information flux, which is a generalization of the signal-to-noise ratio to scenarios where background systematics can no longer be neglected.

In the rest of this section we will present the various components of `swordfish` and show how they are used in practice. Most of the theoretical background can be found in Appendix. A, as well as in our technical paper Ref. [3].

C. Examples I: Variance, Information Flux, Limits and Discovery Reach

For the purpose of demonstrating the various capabilities of `swordfish`, we set up a simple model with two background components, two different signal shapes, a covariance matrix for background uncertainties, and flat exposure. Most of the code is for the construction of

example signal and background spectra.

```
import numpy as np
import swordfish as sf

# Basic grid
x = np.linspace(0, 10, 100)
dx = x[1] - x[0]

# Signal components
S1 = 3.0*np.exp(-(x-5)**2/2.)*dx
S2 = 2.0*np.exp(-(x-6)**2/2.)*dx

# Background components
B1 = 8./x*dx
B2 = 0.3*x*dx

# Background covariance matrix
X, Y = np.meshgrid(x,x)
K = (np.exp(-(X-Y)**2/20.)*0.02**2
      +np.exp(-(X-Y)**2*10.)*0.01**2)

# Exposure
E = np.ones_like(B1)*100.
```

The instantiation of `swordfish` is just a single line, depending only on the various background components and the exposure.

```
# Instantiate Swordfish
SF = sf.Swordfish([B1, B2], T=[0.1, 0.],
                  E=E, K=K)
```

We assumed here that there are two background components (first argument), where the normalization of the first component, B_1 , is uncertain by 10% (second argument). Furthermore, the third and fourth argument describe respectively the exposure and the covariance matrix. Note that this is just a convenient wrapper and that internally the background components and their uncertainties are recast in terms of the total background B and additional contributions to the covariance matrix K .

In Fig. 2 we show for convenience the two signal and background components that we defined above. We also indicate possible realizations of the background variations that are encoded in the covariance matrix K . Furthermore, we illustrate in Fig. 3 the covariance matrix.

a. Covariance and Fisher matrix. The covariance matrix, Σ , of multiple signal components can be calculated by calling the method `covariance`, with a list of signal shapes as argument.

```
# Calculate covariance between multiple
# signal components
print SF.covariance([S1, S2], S0=2*S1)
>> [[ 0.52 -0.60]
      [-0.60  1.16]]
```

More specifically, this corresponds to the covariance matrix for a linear model with $\mathbf{S}(\boldsymbol{\theta}) = \theta_1 \mathbf{S}_1 + \theta_2 \mathbf{S}_2$, around

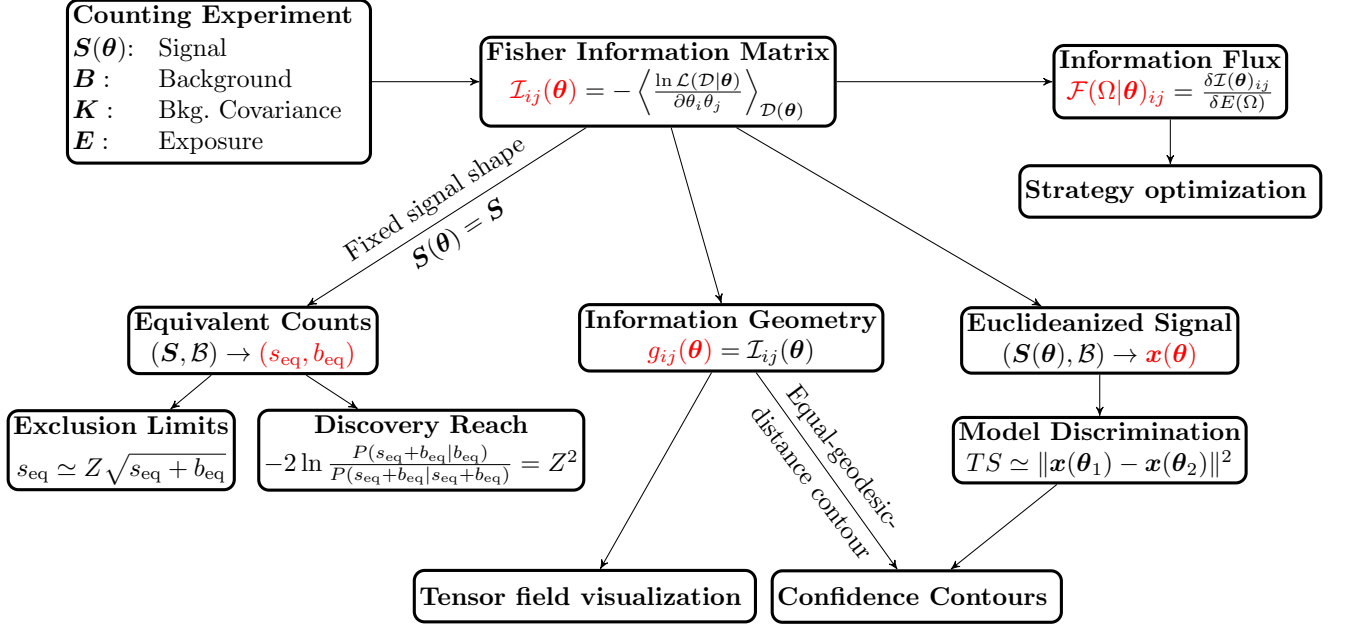


FIG. 1. Overview of the various capabilities of the `swordfish` package. The arrows throughout the diagram indicate the work flow of `swordfish`. Starting with the input in the top left corner, a counting experiment within `swordfish` is completely described by the signal(s), background(s), background covariance, and exposure as defined in Eq. 1. The primary object is the Fisher Information matrix which then allows for the computation of multiple quantities. For exclusion limits and discovery reach we use the Equivalent Counts method described in [3]. Treating the Fisher matrix as a metric on the parameter space then allows for two visualization schemes, adaptive streamlines and traditional confidence contours. We also introduce here a new technique known as the Euclideanized signal for model discrimination in future experiments and as an alternative route to confidence contours in multi-model parameter spaces. Finally, we allow for fast computation of the Information flux, a generalization of the signal to noise ratio, for strategy optimization.

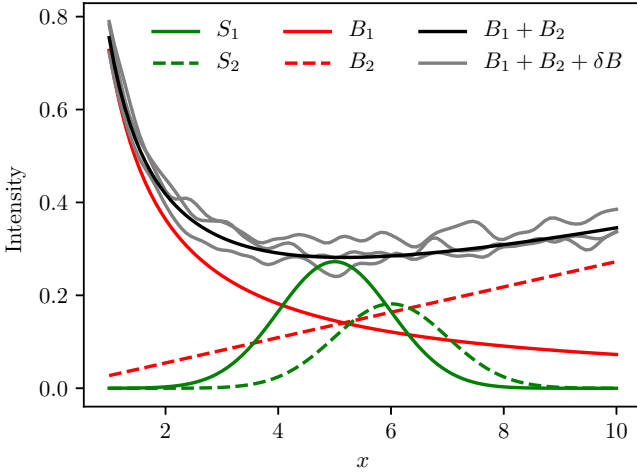


FIG. 2. Possible signal and background components adopted in Example I. We also indicate some realizations of the background uncertainties δB , as they are encoded in the covariance matrix K , by sampling from the corresponding multivariate normal distribution.

values of $\theta_1 = 2$ and $\theta_2 = 0$ (i.e., we assume that there is an additional contribution of $2\mathbf{S}_1$ to the background noise

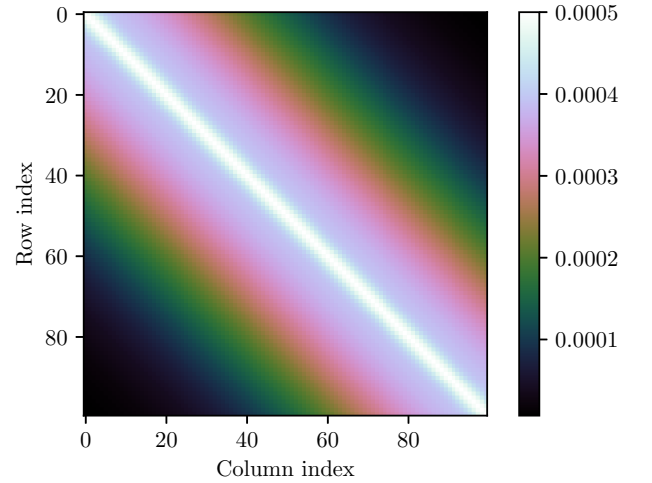


FIG. 3. Illustration of the covariance matrix that we adopted in Example I. It has a narrow component, as well as a weak broad component.

level, which is provided via the keyword argument `S0`). General non-linear models can be handled by numerical differentiation as discussed below in Sec. IID.

Technically, the covariance matrix is derived as matrix

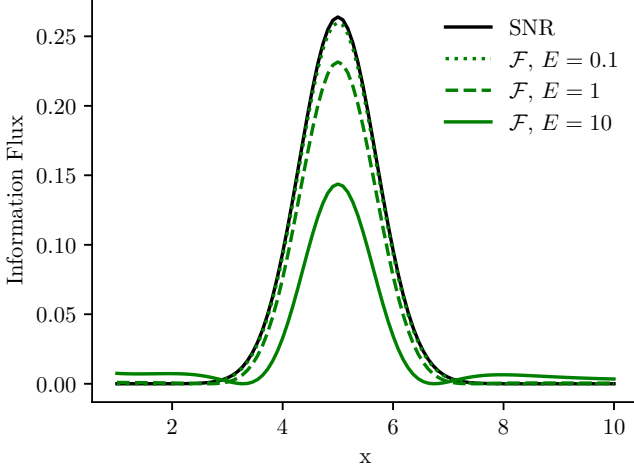


FIG. 4. The signal-to-noise ratio of signal S_1 , compared to the information flux at different values of the exposure E . Here, $E = 1$ corresponds to our baseline model. It is clearly evident that the information flux drops as the measurement enters the systematics dominated regime (for large exposures), and side-bands become more relevant since they facilitate signal background discrimination.

inverse of the Fisher information matrix, \mathcal{I} , which can be obtained using the `fishermatrix` method.

```
# Obtain Fisher information matrix for
# multiple signal componets
print SF.fishermatrix([S1, S2])
> [[ 4.74  2.43]
    [ 2.43  2.11]]
```

Here, we assumed an expansion around $\theta_1 = \theta_2 = 0$, since the default value of S_0 is zero.

b. Information flux. With `swordfish`, it is possible to calculate the *information flux*, which we proposed as a generalization of the common signal-to-noise ratio (SNR) in Ref. [3]. It quantifies how infinitesimal changes of the exposure in each bin affect the variance. We hence define the information flux associated with bin i as the partial derivative of the inverse variance w.r.t. the exposure in the same bin, E_i , namely

$$\mathcal{F}_i \equiv \frac{\partial(1/\sigma^2)}{\partial E_i}. \quad (3)$$

Here, we assume a single-component linear signal model, $\mathbf{S}(\theta) = \theta \mathbf{S}_1$, and $\sigma^2 \equiv \Sigma_{\theta\theta}$. Note that in absence of background uncertainties, this definition simply yields $\mathcal{F}_i = S_i^2/B_i$, which is indeed the conventional SNR.

In `swordfish`, the information flux for a linear one-component signal model can be calculated using the `infoflux` method, providing the signal shape as argument (here, the signal is never added to the background noise).

```
# Obtain information flux
```

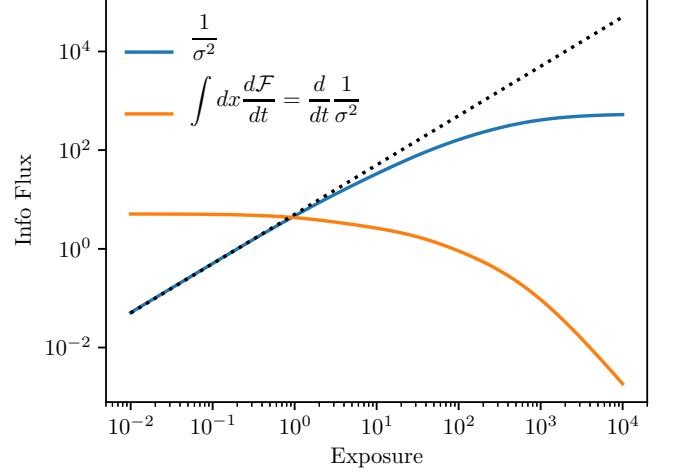


FIG. 5. The inverse variance of the S_1 normalization as function of the exposure. We also show the integrated information flux, which equals the derivative of the inverse variance w.r.t. the exposure.

```
print SF.infoflux(S1)
> [9.7e-04, 9.2e-04, ..., 7.2e-5]
```

The information flux for S_1 is shown in Fig. 4, at different exposure times. It is evident that for short exposure times, where observations are still limited by statistical noise, the information flux equals the SNR. For larger exposure times, however, where the measurement enters the systematics limited regime, the information flux from the main signal region decreases drastically, while the information flux from ‘side-band’ regions becomes enhanced. This is evident in Fig. 4 for exposures above $E \sim 10$.

Summing the information flux over all bins simply yields the exposure derivative of the inverse variance, $d\sigma^{-2}/dE$, if we pretend that the exposure is increased simultaneously in all bins (otherwise the integral should be reweighted accordingly). Integrating this expression from zero to some total exposure gives back the inverse variance as function of that total exposure. This is illustrated in Fig. 5. We indicate also the case where the inverse variance increases linearly with the exposure, as is the case in the statistics-limited regime. Deviations occur for exposures that enter the systematics limited regime.

c. Equivalent counts method. In the Gaussian regime, the (co-)variance of a signal is enough to estimate discovery thresholds and expected upper limits. However, this is not the case closer to the Poisson regime. To obtain accurate results in this case, we adopt the *equivalent counts method* that we developed in Ref. [3]. It is based on the idea that the signal \mathbf{S} , together with the background and its uncertainties defined in some `Swordfish` instance \mathcal{R} , can be mapped on two non-negative numbers,

$$(\mathbf{S}, \mathcal{R}) \rightarrow (s_{\text{eq}}, b_{\text{eq}}) \quad (4)$$

such that the full profile log-likelihood ratio, is approximated by the log-Poisson likelihood ratio,

$$-2 \ln \frac{\mathcal{L}_p(\mathcal{D}_A(\mathbf{S}_0)|\mathbf{S}_0)}{\mathcal{L}_p(\mathcal{D}_A(\mathbf{S}_0)|\mathbf{S})} \simeq -2 \ln \frac{P(b_{\text{eq}}|b_{\text{eq}})}{P(b_{\text{eq}}|s_{\text{eq}} + b_{\text{eq}})} . \quad (5)$$

Here, $\mathcal{D}_A(\mathbf{S})$ refers to ‘Asimov data’ [1], where we set $d_i = \mu_i(\mathbf{S}, \delta\mathbf{B} = 0)$, and $\mathbf{S}_0 \equiv 0$ corresponds to a vanishing signal. This leads to median expected limits and discovery thresholds. We will show the numerical validity of this approximation in the appendix B. Based on the Poisson likelihood ratio, it is then possible to derive accurate estimates for the discovery reach and expected exclusion limits.

For a single-component linear signal, $\mathbf{S}(\theta) = \theta\mathbf{S}$, we define the *equivalent number of expected signal and background counts* as,

$$s_{\text{eq}}(\theta) \equiv \frac{\theta^2}{\sigma^2(\theta) - \sigma^2(\theta_0)} , \quad (6)$$

and

$$b_{\text{eq}}(\theta) \equiv \frac{\theta^2 \sigma^2(\theta_0)}{[\sigma^2(\theta) - \sigma^2(\theta_0)]^2} , \quad (7)$$

where $\sigma^2 \equiv \Sigma_{\theta\theta}$ like above. When calculating $\sigma^2(\theta)$, the signal is assumed to contribute to the background noise, whereas we used $\theta_0 \equiv 0$ to indicate that the corresponding variance is calculated while setting the signal contribution to the background to zero.

Although probably not obvious on first sight, these expressions lead to the exact number of signal and background events for the single-bin Poisson process. We use them here to generalize the notion of signal and background counts to any complex experiment in the form of Eq. (1). For more detail on the motivation behind these definitions see A3. Validations of the method can be found in Ref. [3].

The equivalent signal and background counts are obtained using the `equivalentcounts` method, with the signal shape as argument.

```
# Obtain equivalent signal
# and background counts
s, b = SF.equivalentcounts(S1)
print s, b
> 6.58 9.15
```

The connection between profile log-likelihood and Poisson likelihood will be discussed further at the end of this subsection. On the other hand, the *total* signal and background counts, summed over all bins, can be calculated with the `totalcounts` method.

```
# Obtain total signal and background
# counts
s, b = SF.totalcounts(S1)
print s, b
> 7.52 33.8
```

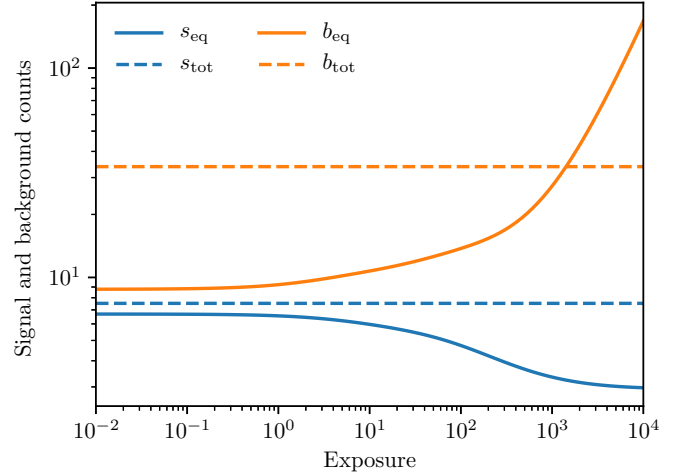


FIG. 6. Equivalent signal and background counts for signal S_1 , as function of the exposure. We clearly see that in the signal and statistics limited regime, the number of equivalent signal and background events is in general less than the total number of signal and background events. This is expected since only events in the most sensitive signal region contribute. However, in the systematics limited regime, the number of equivalent signal events drops further, whereas the increasing number of background events corresponds to the larger systematic error bars.

Before moving on to discuss how the equivalent signal and background can be used for calculating expected upper limits and the discovery reach, we illustrate their behaviour in Fig. 6. Note that the count numbers are divided by the exposure, to emphasize the non-linear parts of the relation. For comparison, we also show the total signal and background counts in the example. The equivalent signal counts are always somewhat lower than the total number of signal event. This is related to the fact that the events in the tails of the signal peak do not effectively contribute to the overall SNR. The number of equivalent signal events furthermore starts to decrease in the systematics dominated regime. On the other hand, the number of equivalent background events is *much* lower than the total number of background events. This comes from the fact that only events around the region where the signal is significant (the ‘signal region’) actually contribute. However, in the systematics-limited regime, the number of equivalent background counts grows significantly. This accounts for the fact that the systematic error does not decrease with additional data. We note that the concept of equivalent signal and background events is a useful because (a) it leads to quantitatively (to within good approximation, see below) correct results for discovery reach and upper limits, and (b) because it provides a notion for estimating how close to the Poisson regime a specific observation actually is.

d. Discovery reach and expected limits. Thanks to the approximate equivalency in Eq. (5), it is enough to consider a one-bin Poisson process. We just have to insert

the equivalent counts as function of signal normalization θ to obtain the desired general results. The *discovery reach* corresponds to the expected number of equivalent signal events, s_{eq} , for which the background-only hypothesis, b_{eq} , can be rejected with a median statistical significance of α . It can be calculated by solving the implicit equation²

$$-2 \ln \frac{P(s_{\text{eq}} + b_{\text{eq}} | b_{\text{eq}})}{P(s_{\text{eq}} + b_{\text{eq}} | s_{\text{eq}} + b_{\text{eq}})} = Z^2, \quad (8)$$

where Z is derived from the inverse of the standard normal cumulative distribution function, denoted F_N , as

$$Z(\alpha) \equiv F_N^{-1}(1 - \alpha). \quad (9)$$

With *swordfish* the discovery reach can be calculated with the `discoveryreach` method which takes, besides the signal shape, the statistical power of the signal discovery, α .

```
# Derive discovery reach
alpha = 2.87e-07 # 5 sigma, one-sided
print SF.discoveryreach(S1, alpha)
> 2.85
```

Conversely, *swordfish* also calculates the expected statistical significance of a given signal. This is done by the `significance` method, which behaves as inverse of the `discoveryreach` method.

```
# Derive stat. significance
print SF.significance(S1*2.85)
>> 2.87e-07
```

Expected upper limits are, in contrast to the discovery reach, conceptually somewhat ambiguous. This is related to the fact that any particular procedure to derive an upper limit from some data implements a compromise between correct coverage, practicality and resilience to downward fluctuations.³ Our procedure to derive an expected $(1 - \alpha)$ CL upper limit is simply to solve the implicit equation

$$s_{\text{eq}} = Z \sqrt{s_{\text{eq}} + b_{\text{eq}}}, \quad (10)$$

where Z is given by Eq. (9) above. For upper limits with 95% or 99.7% CL, the method leads to good results even in the $b_{\text{eq}} \rightarrow 0$ limit, due to some numerical coincidence

² This approach, based on likelihood ratios and $Z(\alpha)$, leads to results that are in rather good agreement with the technically correct treatment which involves partial sums over the Poisson distribution and makes direct connection with the statistical significance α , not $Z(\alpha)$. See Ref. [3] for details.

³ We remind that a puritan's upper limit with perfect coverage behaviour would yield in the case of a strong downward fluctuation the empty set as confidence interval. This is an outcome that experimentalists like to avoid.

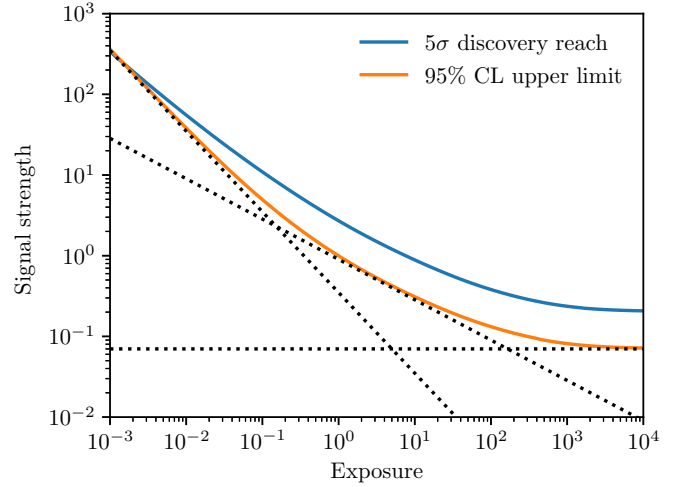


FIG. 7. We show projected upper limits on the signal components S_1 as well as the discovery threshold. The upper limits show clearly the typical behaviour in the signal limited ($\propto E^{-1}$), background limited ($\propto E^{-0.5}$) and systematics limited ($\propto \text{const}$) regime.

which is discussed in Ref. [3]. More specifically, we found that the above procedure leads to results that are in good (usually $< 10\%$, in specific extreme cases up to 40%) agreement with median upper limits that we derived with a fully coverage corrected Monte Carlo for a series of benchmark scenarios.

In *swordfish* the upper limit is calculated by using the `upperlimit` method, providing the significance level as well as the signal shape as arguments.

```
# Derive expected upper limits
alpha = 0.05 # 95% CL
print SF.upperlimit(S1, alpha)
> 0.99
```

In Fig. 7, we show the expected upper limits and discovery reach for signal S_1 as function of the exposure. We also indicate the expected scaling of the upper limit in the signal limited ($\propto E^{-1}$), background limited ($\propto E^{-1/2}$) and systematics limited ($\propto \text{const}$) regimes. These are all reproduced properly.

e. Euclideanized signal method. The model discrimination power of an experiment is often quoted as the significance level z (in terms of standard deviations) at which two benchmark signals S_1 and S_2 can be distinguished. Here, z can be estimated from the expected profile log-likelihood ratio,

$$\text{TS} = -2 \ln \frac{\mathcal{L}_p(\mathcal{D}_A(S_2)|S_1)}{\mathcal{L}_p(\mathcal{D}_A(S_2)|S_2)}, \quad (11)$$

where \mathcal{D}_A denotes again Asimov data as above. Using the Fisher approximation, this TS value can be approximated

by

$$\text{TS} \simeq \sum_{ij} \Delta S_i D_{ij}^{-1} \Delta S_j, \quad (12)$$

where $\Delta \mathbf{S} \equiv \mathbf{S}_1 - \mathbf{S}_2$ is the signal difference, and the total (statistic plus systematic) covariance matrix is given by

$$D_{ij} \equiv K_{ij} + \delta_{ij} \frac{S_{2,i} + B_i}{E_i}. \quad (13)$$

The interpretation of the TS value in units of standard deviations is context dependent. We will give here one very typical example. Suppose \mathbf{S}_1 and \mathbf{S}_2 are part of a parametric signal model, $\mathbf{S}_1 = \mathbf{S}(\boldsymbol{\theta}_1)$ and $\mathbf{S}_2 = \mathbf{S}(\boldsymbol{\theta}_2)$, and that $\boldsymbol{\theta}$ has k relevant components. Furthermore, suppose now that $\boldsymbol{\theta}_1$ are the parameters of the simple null hypothesis that we want to test, and the composite alternative hypothesis that we want to discriminate against is that $\boldsymbol{\theta}$ can acquire any value. The above TS value corresponds then approximately to the median TS value that we would measure in repeated experiments if the true model parameters were $\boldsymbol{\theta}_2$ (we use as data the Asimov data set corresponding to $\boldsymbol{\theta}_2$, in which case the maximum-likelihood estimator of $\boldsymbol{\theta}$ in the alternative hypothesis would be simply $\boldsymbol{\theta}_2$). Since the alternative and null hypothesis are nested, and differ in their degrees of freedom by k , we can assume that the TS value is approximately χ_k^2 distributed, with k degrees of freedom [1, 5]. The corresponding threshold value for a $(1 - \alpha)$ CL contour is then given by

$$Y_k^2(\alpha) = F_{\chi_k^2}^{-1}(1 - \alpha). \quad (14)$$

For instance, in the case of two parameters, $k = 2$, the 68.7%CL or 95.3%CL contours correspond to $Y_{k=2}^2 = 2.32$ and $Y_{k=2}^2 = 6.12$ respectively.

Calculating the pair-wise TS-values for N different signals would require N^2 matrix inversions, which is prohibitive if the number of points is large (say, $N \sim 10^6$, which is not a large number in the context of global scans). The main idea of the *Euclideanized signal method* is to reduce this to just N matrix inversions. To this end, we define the *Euclideanized signal*, which constitutes a mapping of the signal and background onto vectors of length n_b ,

$$(\mathbf{S}_1, \mathcal{B}) \rightarrow \mathbf{x}_1 \quad \text{and} \quad (\mathbf{S}_2, \mathcal{B}) \rightarrow \mathbf{x}_2, \quad (15)$$

such that to good approximation the TS value can be replaced by the Euclidean distance between \mathbf{x}_1 and \mathbf{x}_2 ,

$$\text{TS} \simeq \|\mathbf{x}_1 - \mathbf{x}_2\|^2. \quad (16)$$

The mapping depends on the specific noise level of the background as well as the specified background uncertainties. It is defined in the appendix, Eq. (A18). Here, we just list a few limiting cases. In the background-limited regime where systematics are neglected, we have

$x_i \simeq S_i \cdot \sqrt{E_i/B_i}$. In the systematics limited regime, the expression looks like $x_i = \sum_j (K^{-1/2})_{ij} S_j$. In both cases, the signal enters just linearly, since it does not contribute to the background noise. This is however different in the signal limited regime, which requires some extra care. In this limit, we obtain $x_i \simeq 2\sqrt{E_i S_i}$, where the 2 is a fudge factor that compensates for the fact that only the square-root of the signal appears. However, one can show that the latter implies to lowest order in $\Delta S_i/\sqrt{\bar{S}_i}$ that $\text{TS} \approx \sum_i \Delta S_i^2/\bar{S}_i$, with $\bar{\mathbf{S}} \equiv \frac{1}{2}(\mathbf{S}_1 + \mathbf{S}_2)$. We show in appendix B for a series of randomized models that the mapping works accurately enough for typical applications.

In swordfish, this mapping is implemented in the `euclideanize` method. The TS-value between the signals \mathbf{S}_1 and \mathbf{S}_2 can be then calculated as shown in the following example.

```
# Euclideanized signal
x1 = SF.euclideanize(S1)
x2 = SF.euclideanize(S2)
TS = ((x1 - x2)**2).sum()
# This is the same as:
# TS = SF.TS(S1, S2)
print TS
>> 1.38
```

f. Profile log-likelihood. In order to double-check the accuracy of the equivalent counts and equivalent signal methods, swordfish provides a method to calculate the profile likelihood in Eq. (1) directly. This is done by calling the method `lnL`, which returns the value of the profile log-likelihood, $\ln \mathcal{L}_p(\mathcal{D}_A(\mathbf{S}_0)|\mathbf{S}_1)$. Internally, this profile log-likelihood is maximized w.r.t. the background perturbations $\delta \mathbf{B}$ by using the L-BFGS-B algorithm [6]. In the following example we calculate a profile likelihood ratio, and compare it with the results from the equivalent counts and the Euclideanized signal approximations.

```
# Exact profile log-likelihood ratio
S0 = np.zeros_like(S1) # Zero signal
TS_L = -2*(SF.lnL(S0, S1)
          -SF.lnL(S0, S0))

# Poisson likelihood ratio,
# using equivalent counts
s, b = SF.equivalentcounts(S1)
TS_P = 2*(s-b*np.log((s+b)/b))

print TS_L, TS_P
> 3.28 3.25
```

```
# Exact profile log-likelihood ratio
TS_L = -2*(SF.lnL(S1, S2)
          -SF.lnL(S1, S1))

# Euclideanized signal
x1 = SF.euclideanize(S1)
```



```
x2 = SF.euclideanize(S2)
TS_E = ((x1-x2)**2).sum()
print TS_L, TS_E
> 1.43 1.38
```

We find that for these specific cases the results are in good agreement with each other. Comparisons with a large number of randomized models can be found in appendix B.

D. Examples II: Information Geometry, Confidence Contours, Distance sampling, Validation

All examples in the previous subsection were related to signals with a fixed shape and free normalization. However, often signals have a general parametric form. `swordfish` provides several methods to handle parametric signals. The typical use case is to derive projected confidence contours.

As an example signal for this subsection, we define a periodic signal with two parameters for the normalization, a , and for the phase offset, b , respectively.

```
# Parametric signal
S = lambda a, b:
    b*np.sin(x+0.5*a+0.1*b)**2*dx
```

a. Covariance and Fisher matrix. Parametric signal shapes can be handled by the methods `fishermatrix` and `covariance`, provided they are linearized before by using the method `linearize`. This can happen for instance by numerical differentiation. Estimating the covariance of the above model parameters a and b can then be done as shown in the following example.

```
# Calculation of covariance matrix
a0, b0 = 2, 6
gradS, S0 = SF.linearize(S, [a0, b0])
print SF.covariance(gradS, S0 = S0)
>> [[0.26, -0.50], [-0.50, 2.44]]
```

This method cannot be used if higher-order derivatives of the signal play a significant role. In that case, some of the methods that we discuss in the following section can be used instead.

b. Information geometry and confidence contours. The Fisher information matrix defines a *metric* on the space of model parameters (which is the topic of *information geometry*). Expected confidence regions for parameter reconstruction happen to correspond to equal-geodesic-distance contours w.r.t. this metric. `swordfish` provides methods to construct confidence contours by internally solving the geodesic equation. However, it also provides a more general way of visualizing the Fisher information metric using adaptive-density streamlines. In some sense, the streamline visualization represents all possible confidence contours simultaneously, and is hence more general.

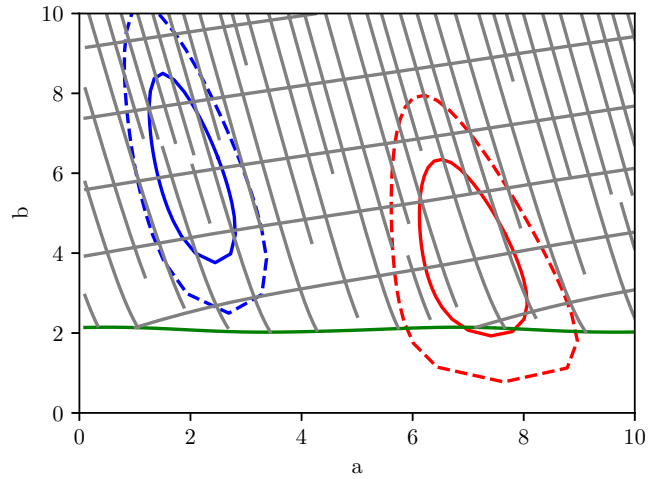


FIG. 8. *Gray lines:* Visualization of the Fisher information metric, using streamlines. The line orientation corresponds to the major and minor axes of the Fisher information metric (or covariance matrix). The line density changes such that the distance between parallel lines is $\sim 1\sigma$ (see text for details). A larger signal normalization b enables a better reconstruction of the signal position a . *Red and blue lines:* Equal geodesic distance contours, representing expected 1σ and 2σ confidence regions. Note that the confidence regions constructed with this local method do *not* account for the periodic structure of the example signal model, which actually leads to disconnected confidence regions (see Fig. 9 for comparison). *Green line:* Expected exclusion limits on b (for fixed a) at 95%CL.

The Fisher information metric defines a tensor field, which can be generated by using the `getfield` method. This method, as well as the visualization methods, are currently only implemented for signal models with two parameters. It takes as arguments the signal model, as well as the two lists that specify the grid on which the tensor field is evaluated.

```
# Generation of tensor field
alist = np.linspace(0.1, 10, 40)
blist = np.linspace(0.1, 10, 40)
TF = SF.getfield(S, alist, blist)
```

Based on the tensor field, confidence contours can be generated using the `contour` method, which takes as argument both the central point of the contours as well as a distance.

```
# Confidence contour visualization
# (equal geodesic distance contours)
a0, b0 = 6, 2 # center
d = 2.32 # distance
TF.contour([a0, b0], d, color='red')
```

This code generates a confidence contour with geodesic distance $d = 2.32$ around the indicated central point (a_0, b_0) . This corresponds to a 68.3%CL region. Examples for confidence contours generated this way are shown in Fig. 8

Internally, the method first generates Christoffel symbols by numerical differentiation of the tensor field. Second, it shoots geodesics of the specified length from the central point in a number of directions, and finally connects the endpoints. More details can be found in appendix A 4 b.

Instead of showing confidence contours for specific benchmark points, it is also useful to directly visualize the underlying Fisher information metric field. In fact, this can lead to a more complete, although somewhat unusual, representation of experimental abilities than specific confidence contours could do. A large number of visualization techniques exist for tensor fields [7]. In *swordfish*, we implemented some variation of adaptive-density streamline visualization (e.g., Ref. [8]) which works for 2-dim parameter spaces.

Adaptive-density streamline plots are straightforward to interpret: The direction of the streamlines corresponds exactly to the major and minor axes of the Fisher information metric (and hence of the covariance matrix). The distance between two parallel streamlines corresponds *approximately* to 1σ in the direction perpendicular to the streamlines. The latter condition is realized by adding or removing lines as necessary.

In *swordfish*, streamlines are generated by first generating `VectorField` objects from the tensor field, using the `VectorFields` method. Streamlines are then generated with the method `streamlines`. An example is shown in Fig. 8.

```
# Streamline visualization
vf1, vf2 = tf.VectorFields()
vf1.streamlines(color='0.5')
vf2.streamlines(color='0.5')
```

The streamline generation is an iterative process. First, two perpendicular streamlines are drawn starting from a seed location. Starting from random points on the existing streamlines, it is then checked whether a parallel line at around 1σ distance exists. If not, it is added and extended until it gets too close to an already existing streamline. Further details can be found in appendix A 4.

c. Sampling and confidence contours. The above visualization of confidence contours using equal geodesic distance contours is a local method, and hence does not correctly treat multi-modal confidence regions. Furthermore, it would break down when the Fisher information matrix is singular, which often happens for high-dimensional models that are not sufficiently constrained by data.

In the following example, we first generate a distance field using the TS method, which adopts the above Euclideanized signal method to approximate the profile log-likelihood.

```
# Confidence contour visualization
# (distance measure sampling)
a0, b0 = 3, 5
```

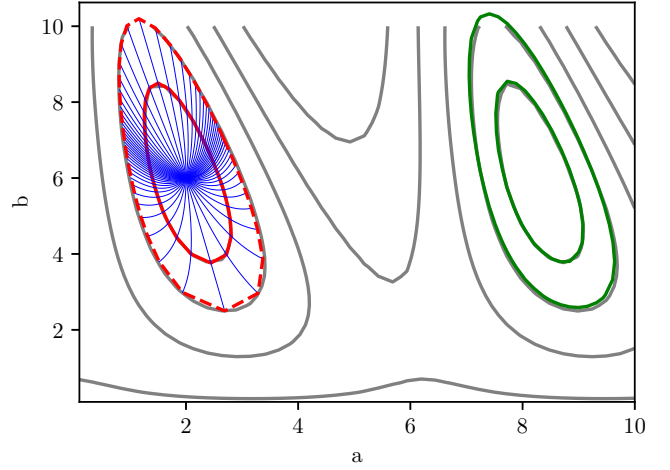


FIG. 9. *Gray lines:* Confidence contours constructed by using the equivalent shape method, which also works for multi-model confidence regions. *Red lines:* Confidence regions from the equal geodesic distance contours (the blue lines show the geodesics used for constructing this region). *Green lines:* Confidence regions constructed using the minuit algorithm of `minuit`.

```
Sd = S(a0, b0)
TSfield = np.array([[SF.TS(S(a,b), Sd)
                     for a in alist] for b in blist])
plt.contour(alist, blist, TSfield**0.5,
            levels = [1, 2, 3], colors='0.5')
```

The resulting contours are shown in Fig. 9. They correctly account for the multi-modal structure of the confidence contours, and agree with the geodesic distance contours where they overlap.

d. Validation with numerical likelihood maximization. In particle and astroparticle physics, a very common approach to handling profile log-likelihoods and related inference problems is to make use of the C++ numerical minimizer `minuit`. In order to validate the approximation schemes used in *swordfish*, it is for any given model possible to directly generate a `Minuit` instance (part of the Python package `iminuit`). This can then be used to derive confidence contours etc and compare with *swordfish* results. This is done using the factory method `getMinuit`, where as arguments the parametric signal as well as the true signal parameters have to be provided. Note that the profiling over background perturbations, $\delta\mathbf{B}$, is done not by `minuit` but by calling L-BFGS-B, as described above for the `lnL` method (L-BFGS-B directly uses analytic gradient information, which leads to a very significant speed-up). In the following example, we show how confidence contours can be generated with `Minuit`.

```
# Generate Minuit instance
# of Swordfish model
a0, b0 = 6, 2
M = SF.getMinuit(S, [a0, b0])
```

```

M.migrad()
M.minos()
X, Y, TSfield = M.contour(
    "x0", "x1", bound = 3.)
TSfield = np.array(TSfield)
TSfield -= TSfield.min() # zero
plt.contour(X, Y, TSfield**0.5,
    levels=[1, 2, 3], colors='green')

```

The resulting contours are shown in Fig. 9, and agree with contours generated using the geodesic equation or the distance sampling method.

III. PHYSICS EXAMPLES

We will now discuss two typical examples from direct and indirect searches for dark matter signals. The main purpose of these examples is to illustrate how the various possible inputs of `swordfish` connect to physical fluxes and the exposure, and how various statements about model parameters can be derived in practice. Our goal was to keep the examples as simple as possible, and not to exactly reproduce published results. However, all observed deviations can be entirely attributed to the different physics assumptions that are made. We showed already above that `swordfish` reproduced results obtained from the profile-likelihood method.

A. Galactic center dark matter searches with a CTA-like experiment

Our first example is inspired by the upcoming Cherenkov Telescope Array (CTA), and we will largely follow a simplified version of the ON-OFF analysis discussed in Ref. [9]. The idea is to measure the gamma-ray intensity in a ‘ON’ region close to the Galactic center, and to compare it with the intensity in an ‘OFF’ region that is somewhat further away. If no difference in the intensity is observed, upper limits on a dark matter contribution (which would predominantly contribute to the ON region) can be obtained.

We assume throughout dark matter annihilation into $\bar{b}b$ final states, and an Einasto profile and ON/OFF regions with the same parameters as assumed in Ref. [9]. The J-values and the angular size of these regions are: $J_{\text{ON}} = 21 \times 10^{21} \text{GeV}^2 \text{cm}^{-5}$, $J_{\text{OFF}} = 21 \times 10^{21} \text{GeV}^2 \text{cm}^{-5}$, $\Omega_{\text{ON}} = 3.2 \times 10^{-3}$, and $\Omega_{\text{OFF}} = 3.2 \times 10^{-3}$. The cosmic-ray electron background is assumed to follow a broken power law $dN_{e^-}/dE = 1.17 \times 10^{-11} \left(\frac{E}{\text{TeV}}\right)^{-\Gamma} \text{cm}^{-2} \text{s}^{-1}$, where $\Gamma = 3.0$ for $E < 1 \text{ TeV}$, and $\Gamma = 3.9$ for $E > 1 \text{ TeV}$. The cosmic-ray proton flux is assumed to follow a power law $dN_p/dE = 8.73 \times 10^{-9} \left(\frac{E}{\text{TeV}}\right)^{-2.71} \text{cm}^{-2} \text{s}^{-1}$, and we assume a 99% rejection efficiency and a factor 3 shift in energy for reconstructed protons (see Ref. [9] for details). The Galactic diffuse emission is neglected

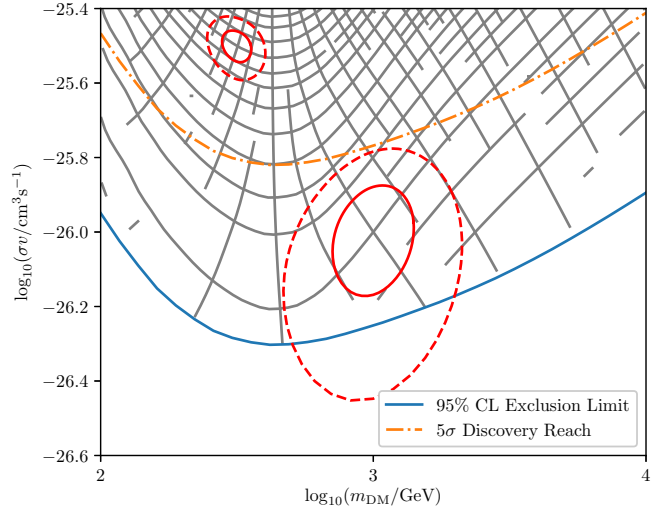


FIG. 10. Blue solid line and orange dot-dashed show the 95%CL exclusion limit and 5σ discovery reach respectively. We also plot two examples of 1σ and 2σ contours. The grey lines are 1σ streamline visualisation, as described in the previous sections.

for simplicity (although it likely *does* play a significant role, and should not be neglected in any real analysis or projection). We sum both electron and proton contributions to a single isotropic component, and assume that its normalization is uncertain by 50%, but identical in both the ‘ON’ and ‘OFF’ regions. Besides that, we do not adopt any additional systematic background uncertainties. Lastly, we adopt the same exposure (now somewhat outdated) curves as in Ref.[9].

The actual implementation of the present example can be found in the `jupyter` notebook `swordfish_ID.ipynb`. In Fig. 10, we show the 95%CL projected upper limits, the 5σ discovery threshold, example reconstruction contours (68.3% and 95.4% CL), as well as the streamline visualization of the Fisher information metric. As it is clear from the code, all this is relatively straightforward to obtain once the instrumental details are coded up.

B. Xenon-1T

Direct detection experiments have, over the past few years, gained several orders of magnitude in sensitivity over a wide range of DM masses. Sensitivity at multiple mass scales is achieved mainly through the use of different target elements allowing various detectors to probe from keV to GeV recoil energies. The use of many smaller scale direct detection experiments with low backgrounds have been discussed in the literature recently [10] providing excellent motivation for a fast and simple way calculate the sensitivity of these future experiments given a physical dark matter model. Direct detection experiments have, over the past few years, gained several or-

ders of magnitude in sensitivity over a wide range of DM masses. Sensitivity at multiple mass scales is achieved mainly through the use of different target elements allowing various detectors to probe from keV to GeV recoil energies. The use of many smaller scale direct detection experiments with low backgrounds have been discussed in the literature recently [10] providing excellent motivation for a fast and simple way calculate the sensitivity of of these future experiments given a physical dark matter model. We here implement a simplified calculation of the sensitivities for the Xenon-1T experiment.

The Xenon collaboration have recently published their latest results from 35636 kg days of exposure [11]. The only way to reasonably replicate the results of Ref. [11] is to fully simulate the detector response and signal, tuning your parameters to fit the few number of events in the signal region. Here, we instead calculate the signal distributed over only the primary photon signal (S1). Since Fig. 3 of Ref. [11] provides the background components as a function of S1 we are able to directly extract these and consider how our DM signal would be distributed in the same plane. Typically a DM signal in a DD experiment is expressed as a recoil spectrum given by

$$\frac{dR}{dE_R} = \frac{\rho_0 \xi_T}{2\pi m_{\text{DM}} (2m_T E_R + m_{\text{med}}^2)^2} \eta(v_{\text{min}}(E_R)) , \quad (17)$$

where ρ_0 is the dark matter density at earth which we take to be 0.3 GeV cm^{-3} , m_{DM} is the dark matter mass, m_{med} is the mediator mass, $F_T^2(E_R)$ is the recoil form factor, and m_T is the mass of the target isotope. We use a common approximation $F_T^2(E_R) = \exp(-(r_n \sqrt{2m_T E_R})^2/3)$ for the recoil form factor [12]. To match the known backgrounds as a function of S1 we use the change of variables $\frac{dR}{dS1} = \frac{dR}{dE_R} \frac{dE_R}{dS1}$, for which we need a reasonable approximation of $\frac{dE_R}{dS1}$.

For our approximation we take red line in the bottom panel of Fig. 2, Ref. [11], to give us the median expected value for the S2 component given a value of S1. We then assume that the points at which the contour lines of constant energy cross the median expected value of S2 approximately describe the typical recoil energy for a given S1. We simply compute the derivative and use the the nuclear recoil efficiency from Fig. 1 along with a factor of 0.475 to take into account the fact that we are only interested in signals in the reference region.

To check our approximation we integrate over the entire distribution of S1 (3 – 70 PE) for the benchmark scenario presented in Ref. [11], namely a 50 GeV DM particle with $\sigma = 10^{-46} \text{ cm}^2$. Our approximation agrees well with the 0.82 presented, finding that we get 0.83 events in the reference region⁴. Note here we take $\sigma = \frac{g^2 \mu}{\pi m_{\text{med}}^4}$

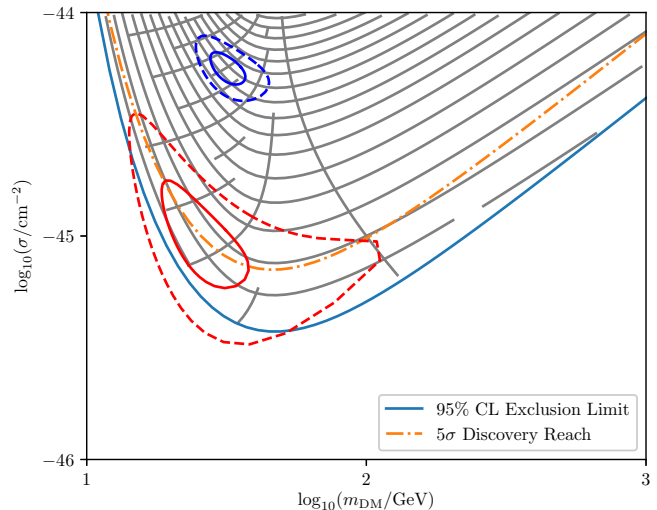


FIG. 11. Blue solid line and orange dot-dashed show the 95%CL exclusion limit and 5σ discovery reach respectively. We also plot two examples of 1σ and 2σ contours. The grey lines are 1σ streamline visualisation, as described in the previous sections.

where $\mu = \frac{m_{\text{DM}} m_p}{m_{\text{DM}} + m_p}$ and m_p is the mass of the proton. Through the same procedure we sum the backgrounds and compare our total signal in the reference region which we find to be 0.37 events, in good agreement with the reported 0.36 events. We simply assume a background uncertainty of 10% for all components separately.

Again, the implementation of the present example can be found in the `jupyter` notebook `swordfish_DD.ipynb`. In Fig. 11, we show the 95%CL projected upper limits, the 5σ discovery threshold, example reconstruction contours (68.3% and 95.4% CL), as well as the streamline visualization of the Fisher information metric. As it is clear from the code, all this is relatively straightforward to obtain once the instrumental details are coded up.

IV. CONCLUSIONS

We introduced `swordfish`, a set of new statistical tools and their implementation in a `Python` package to efficiently forecast and analyse experimental sensitivities in particle and astroparticle physics. Internally, `swordfish` is built on the Fisher information formalism and several new extensions that were introduced here or recently in Ref. [3]. This allows one to skip the often time-intensive Monte Carlo step when performing sensitivity forecasts, and to look at experimental abilities in new and more fine-grained ways. The tool can be immediately applied to many practical problems, as we demonstrate with typical forecasting examples from indirect and direct dark matter searches (the code examples can be found here at github.com/cweniger/swordfish).

The statistical model that we implemented in `swordfish` is a Poisson likelihood function, profiled over general

⁴ To compare with the results of the Xenon1T collaboration we took the mass of the mediator to be very large so it no longer plays a role, $m_{\text{med}} = 10^5 \text{ MeV}$

Gaussian background perturbations. Non-linear signal models are supported. This set-up is generic enough to capture the relevant aspects of a very large number of experiments and signal types relevant for particle physics, astroparticle physics and astronomy (including, for example, collider experiments, direct dark matter searches, radio telescopes, gamma-ray detectors, neutrino detectors, many searches for axion-like particles, and even the analysis of gravitational wave forms).

In *swordfish*, we implement several new statistical methods and efficient approximation techniques.

- *Equivalent counts method.* This approximation technique maps complex signal and background models onto just two numbers: the *equivalent signal* and *equivalent background* counts. These provide information about the number of statistically relevant signal and background events, and are used to quickly derive approximate (but accurate) *discovery thresholds* and *expected upper limits* on the signal flux.
- *New visualization of parameter degeneracies.* The commonly shown expected confidence regions of benchmark signal models have a geometric interpretation as equi-geodesic-distance contours of an underlying information metric. This information metric captures all possible benchmark models *at once*. We introduce an intuitive variable-density streamline visualization of this information metric as a new way to visualize experimental abilities in a benchmark-free way.
- *Fisher information flux.* In absence of systematic uncertainties, the commonly used signal-to-noise ratio is a faithful measure to identify the most sensitive region-of-interest in event space. We generalize this concept to also account for systematic background uncertainties. The resulting *Fisher information flux* can be used for *optimal experimental*

design in situations where background uncertainties cannot be ignored.

- *Euclideanized signal method.* It is often of interest to quantify by how much future experiments will be able to discriminate different parts of a signal parameter space. If the parameter space is high-dimensional, this might require the pair-wise comparison of more than 100 million parameter points. This can be, in principle, achieved with modern clustering algorithms that work in Euclidean space. In *swordfish* we implemented a new way to map signals on their Euclidean analog, such that the Euclidean distance between two signals approximates (with high accuracy) the statistical difference between the model parameter points.

We presented short code examples for how all of the above methods can be easily used for a specific background and signal model. The approximation techniques usually work to within 10%–20%, and are validated in Ref. [3] or in the present work. We finally, showed two simple real-physics examples from both indirect and direct dark matter detection to illustrate the ease of computation and utility of the method. Firstly, the sensitivity to TeV scale annihilating WIMP dark matter with a CTA-like instrument was calculated, following [9]. Secondly, we constructed a simplified version of the Xenon1T experiment using an approximate 1-D analysis using the background signals presented in Ref. [11]. For both examples we showed our visualisation schemes as a unique way to view the model parameter space.

ACKNOWLEDGMENTS

TE would like to greatly thank Bradley Kavanagh for discussions on the Xenon1T signal calculation. We are also happy to thank Jan Conrad, Kyle Cranmer, Pat Scott and Roberto Trotta for useful discussions. This research is funded by NWO through the Vidi research grant 680-47-532.

-
- [1] G. Cowan, K. Cranmer, E. Gross, and O. Vitells, Eur. Phys. J. **C71**, 1554 (2011), [Erratum: Eur. Phys. J. **C73**, 2501(2013)], arXiv:1007.1727 [physics.data-an].
 - [2] H. Cramér, *Mathematical Methods of Statistics (PMS-9)*, Vol. 9 (Princeton university press, 2016).
 - [3] T. D. P. Edwards and C. Weniger, (2017), arXiv:1704.05458 [astro-ph.IM].
 - [4] D. R. Cox, Journal of the Royal Statistical Society. Series B (Methodological) **17**, 129 (1955).
 - [5] S. S. Wilks, The Annals of Mathematical Statistics **9**, 60 (1938).
 - [6] J. L. Morales and J. Nocedal, ACM Transactions on Mathematical Software (TOMS) **38**, 7 (2011).
 - [7] D. H. Laidlaw and J. Weickert, *Visualization and Processing of Tensor Fields: Advances and Perspectives* (Springer Science & Business Media, 2009).
 - [8] K.-F. Tchou, J. Dompierre, M.-G. Vallet, and R. Camarero, (2004).
 - [9] H. Silverwood, C. Weniger, P. Scott, and G. Bertone, JCAP **1503**, 055 (2015), arXiv:1408.4131 [astro-ph.HE].
 - [10] M. Battaglieri *et al.*, (2017), arXiv:1707.04591 [hep-ph].
 - [11] E. Aprile *et al.* (XENON), Phys. Rev. Lett. **119**, 181301 (2017), arXiv:1705.06655 [astro-ph.CO].
 - [12] J. Lewin and P. Smith, Astroparticle Physics **6**, 87 (1996).

Appendix A: Definitions and Derivations

Here we gather all the definitions required to understand the **swordfish** package. We avoid reproducing all the derivations of Ref. [3] and refer there for a more complete set of information.

1. Fisher information matrix

In general, the Fisher information matrix is, given some regularity conditions, defined via the second derivative of the log-likelihood,

$$\mathcal{I}_{kl}(\boldsymbol{\eta}) = - \left\langle \frac{\partial^2 \ln \mathcal{L}(\mathcal{D}|\boldsymbol{\eta})}{\partial \eta_k \partial \eta_l} \right\rangle_{\mathcal{D}(\boldsymbol{\eta})}, \quad (\text{A1})$$

where the average is taken over data realizations of a model with parameters $\boldsymbol{\eta}$. If we apply this definition to the model in Eq. (1), with $\boldsymbol{\eta} = (\boldsymbol{\theta}, \boldsymbol{\delta B})$, we obtain the various Fisher matrix components

$$\mathcal{I}_{\theta_k \theta_l}(\boldsymbol{\theta}) = \sum_i \frac{\partial S_i}{\partial \theta_k} \frac{E_i}{S_i(\boldsymbol{\theta}) + B_i} \frac{\partial S_i}{\partial \theta_l}, \quad (\text{A2})$$

$$\mathcal{I}_{\delta B_k \delta B_l}(\boldsymbol{\theta}) = \delta_{kl} \frac{E_k}{S_k(\boldsymbol{\theta}) + B_k} + K_{kl}^{-1}, \quad (\text{A3})$$

$$\mathcal{I}_{\theta_k \delta B_l}(\boldsymbol{\theta}) = \mathcal{I}_{\delta B_l \theta_k}(\boldsymbol{\theta}) = \frac{\partial S_l}{\partial \theta_k} \frac{E_l}{S_l(\boldsymbol{\theta}) + B_l}. \quad (\text{A4})$$

Here, we assumed that the mock data is generated for $\boldsymbol{\eta} = (\boldsymbol{\theta}, 0)$.

The inverse of the Fisher matrix provides information about the covariance of the parameters. However, we are here not interested in the covariance of $\boldsymbol{\delta B}$. It is hence useful to consider some partially inverted, or *profiled* Fisher information matrix. More specifically, the above Fisher information matrix has block form,

$$\mathcal{I}_{\boldsymbol{\eta}\boldsymbol{\eta}} = \begin{pmatrix} \mathcal{I}_{\boldsymbol{\theta}\boldsymbol{\theta}} & \mathcal{I}_{\boldsymbol{\theta}\boldsymbol{\delta B}} \\ \mathcal{I}_{\boldsymbol{\delta B}\boldsymbol{\delta B}} & \mathcal{I}_{\boldsymbol{\delta B}\boldsymbol{\theta}} \end{pmatrix}. \quad (\text{A5})$$

The ‘profiled Fisher information’ matrix for parameters $\boldsymbol{\theta}$ only is then given by

$$\mathcal{I} = \mathcal{I}_{\boldsymbol{\theta}\boldsymbol{\theta}} - \mathcal{I}_{\boldsymbol{\theta}\boldsymbol{\delta B}} \mathcal{I}_{\boldsymbol{\delta B}\boldsymbol{\delta B}}^{-1} \mathcal{I}_{\boldsymbol{\delta B}\boldsymbol{\theta}}. \quad (\text{A6})$$

One can now show (see Ref. [3]) that this expression can be written in the simple form

$$\mathcal{I}_{lk}(\boldsymbol{\theta}) = \sum_{ij} \frac{\partial S_i}{\partial \theta_k} D_{ij}^{-1} \frac{\partial S_j}{\partial \theta_l}, \quad (\text{A7})$$

where D is given by

$$D_{ij} = K_{ij} + \delta_{ij} \frac{S_i(\boldsymbol{\theta}) + B_i}{E_i}. \quad (\text{A8})$$

This is the definition of the Fisher information matrix that is used in **swordfish**.

2. Fisher information flux

A common question in experimental design, or the planning of observation strategies, is how much additional data in different areas of observational parameter space would strengthen the constraints on various model parameters. The naive approach, which is to just consider signal-to-noise ratios, does not take into account degeneracies with other model components or background systematics. The Fisher information matrix provides a useful starting point to find a more general definition of the SNR that takes these effects into account.

We define the Fisher information flux as the partial derivative of the information matrix $\mathcal{I}_{kl}(\boldsymbol{\theta})$ w.r.t. exposure E_m ,

$$\mathcal{F}_{kl,m} \equiv \frac{\partial \mathcal{I}_{kl}}{\partial E_m}. \quad (\text{A9})$$

For the above model, this gives

$$\mathcal{F}_{kl,m} = \sum_{ij} \frac{\partial S_i}{\partial \theta_k} D_{im}^{-1} \frac{S_m(\boldsymbol{\theta}) + B_m}{E_m^2} D_{mj}^{-1} \frac{\partial S_j}{\partial \theta_l}. \quad (\text{A10})$$

Note that in **swordfish**, only a one-dimensional linear model is implemented, although the generalization to multiple dimensions is straightforward (see Ref. [3]).

3. Equivalent counts method

The definition of equivalent signal and background events in Eqs. (6) and (7) can be derived as follows. Consider a one-bin Poisson process and a simple linear model $\mu(\theta) = \theta S + B$. The expected number of signal and background events are given by $s = \theta S$ and $b = B$, respectively. These are related to the Fisher information matrix via $\theta^2 \mathcal{I}_{\theta\theta}(\theta) = s^2/(s+b)$. Evaluating this relation both at $\theta_1 > 0$ and in the limit $\theta \rightarrow 0$ gives two equations. These can be inverted to write the number of signal and background events in terms of the Fisher information matrix. We find $s = \theta^2 (\mathcal{I}_{\theta\theta}^{-1}(\theta) - \mathcal{I}_{\theta\theta}^{-1}(0))^{-1}$ and $b = \theta^2 \mathcal{I}_{\theta\theta}^{-1}(0) (\mathcal{I}_{\theta\theta}^{-1}(\theta) - \mathcal{I}_{\theta\theta}^{-1}(0))^{-2}$. The main idea of the equivalent counts method is now to generalize these exact expressions to arbitrary models of the form Eq. (1). Expected upper limits and discovery thresholds can then be derived using the equivalent counts in a hypothetical one-bin Poisson process, instead of the full model. We showed in Ref. [3] that the equivalent counts method is rather accurate for a large variety of cases. In particular, it is by construction accurate in the deeply Poissonian and Gaussian regimes. For intermediate cases, we found that the obtained limits and thresholds agree with fully coverage-corrected Monte Carlo results to within 10–30%. The most extreme deviations that we could identify occur for projected upper limits, in scenarios with the majority of the signal events are buried under a much larger background and a small amount of signal events in a nearly

background free region dominates the signal significant. In this case, a kind of ‘level-splitting’ of the otherwise discrete Poisson likelihood occurs that can be exploited to obtain somewhat stronger limits than what is possible with a pure Poisson likelihood. In this specific case our projected upper limits are a conservative estimate (see Ref. [3] for some more details).

4. Information Geometry

Confidence regions at $(1-\alpha)$ confidence level (CL) have the property that they cover in repeated experiments the true but unknown value in $(1-\alpha)$ of the cases. They are very commonly derived by studying profile likelihood ratios (see, e.g., Ref. [1]). Simple approximations to the expected confidence regions can be found by assuming that the likelihood function has the parameter dependence of a multi-variate normal distribution (‘Gaussian approximation’). However, the viability of the Gaussian approximation depends on the model parameterization. A more accurate and parametrization invariant estimate of the expected confidence regions is based on the geodesic equation.

a. Gaussian approximation

If the Gaussian approximation applies, the expectation-value of the log-likelihood function has the form

$$-2 \left\langle \frac{\ln \mathcal{L}(\mathcal{D}|\theta')}{\ln \mathcal{L}(\mathcal{D}|\theta)} \right\rangle_{\mathcal{D}(\theta)} = \sum_{ij} (\theta_i - \theta'_i) \mathcal{I}_{ij}(\theta) (\theta_j - \theta'_j) \equiv \chi^2. \quad (\text{A11})$$

The expected confidence region at $(1-\alpha)$ CL, provided that θ has been measured, can be obtained by identifying the parameter region where

$$\chi^2(\theta') \leq Y_k^2, \quad (\text{A12})$$

where Y_k is defined in Eq. 14 and k corresponds to the dimensionality of the parameter space θ .

b. Geodesic approximation

The above construction of confidence contours has a geometric interpretation. The Fisher information matrix induces a *metric* on the parameter space of θ . In fact, a central property of the Fisher information matrix is that it transforms like a metric under reparametrization of the model. This follows directly from the definition in Eq. (A1). The region defined above corresponds then to an equal-geodesic-distance contour with distance Y from the point θ (provided that the Fisher information matrix does not vary significantly within the region of interest). A *parametrization-independent definition* of

confidence regions can be found by constructing equal-geodesic-distance contours by solving the geodesic equation,

$$\frac{d^2 \theta_i}{ds^2} + \frac{1}{2} \mathcal{I}_{ij}^{-1} \left(\frac{\partial \mathcal{I}_{lj}}{\partial \theta_k} + \frac{\partial \mathcal{I}_{kj}}{\partial \theta_l} - \frac{\partial \mathcal{I}_{kl}}{\partial \theta_j} \right) \frac{d\theta_k}{ds} \frac{d\theta_l}{ds} = 0. \quad (\text{A13})$$

Although this *geodesic approximation* to confidence contours is still not exact, we find that they in general agree very well with results from traditional likelihood-ratio explorations, both in the statistics and systematic limited regime.

5. Euclideanized signal

The entire point of the ‘euclideanized signals’ that we introduce in this work to enable the rapid calculation of the expected TS value in Eq. (A14) for a *very* large number of signal combinations (e.g., $\sim 10^{16}$ in the case of a Bayesian scan with 100 million points). This would be possible if the most efficient clustering algorithms, which can handle billions of points, can be used. These, however, happen to work in Euclidean space. The goal is hence to map signals \mathbf{S} onto vectors \mathbf{x} such that the TS value is approximately given by the L2-norm in Euclidean space, $\text{TS} \simeq \|\mathbf{x}_1 - \mathbf{x}_2\|^2$.

We start by approximating the TS-value in Eq. (A14) by using the Fisher information matrix evaluated at the mean signal $\bar{\mathbf{S}} = \frac{1}{2}(\mathbf{S}_1 + \mathbf{S}_2)$,

$$\text{TS} \simeq \Delta \mathbf{S}^T D_{\bar{\mathbf{S}}}^{-1} \Delta \mathbf{S}, \quad (\text{A14})$$

where $\Delta \mathbf{S} \equiv \mathbf{S}_1 - \mathbf{S}_2$ denotes the signal difference, and $D_{\bar{\mathbf{S}}}$ corresponds to Eq. (13) with $S_i \rightarrow \bar{S}_i$. If we define now the vector

$$x'_i \equiv \sum_j (D^{-1/2})_{ij} S_j E_j, \quad (\text{A15})$$

it is straightforward to show that it satisfies

$$\text{TS} \simeq \|\mathbf{x}'_1 - \mathbf{x}'_2\|^2 \quad \text{if} \quad D_{\mathbf{S}_1} \approx D_{\mathbf{S}_2}. \quad (\text{A16})$$

However, in the case where the shot noise of the signal has a significant impact on the total background uncertainties, the above relationship will break down. This becomes actually a large effect in the strong-signal limit. In fact, to second order in ΔS_i^2 , we find that

$$\|\mathbf{x}'_1 - \mathbf{x}'_2\|^2 \approx \frac{1}{4} \sum_i \frac{\Delta S_i^2}{\bar{S}_i} \quad \text{if} \quad \bar{S}_i \gg B_i + E_i K_{ii}. \quad (\text{A17})$$

Hence, we would in this limit underestimate the discrimination power of an instrument systematically by a factor of two. In order to avoid this problem, we multiply \mathbf{x}' with some *fudge factor* that equals one for negligible signals, and equals two when the signal dominates. We will

show below that this procedure leads to satisfactory results.

The above discussion motivates the definition of the ‘Euclideanized signal’,

$$x_i \equiv \left(\sum_j (D^{-1/2})_{ij} S_j E_j \right) \left(1 + \frac{R \cdot S_i}{R \cdot S_i + B_i + K_{ii} E_i} \right), \quad (\text{A18})$$

where we take the weight $R = 0.1$, which we found to lead to the best results. It has the property that the TS-value corresponding to two signals can now be written as Euclidean distance between their euclideanized signal vectors, as shown in Eq. (A14).

In order to test the accuracy of the above procedure, we randomly generated a large number of models with $n_b = 10$, using randomized signals \mathbf{S} and randomized covariance matrices K . Without loss of generality, the background and the exposure are kept flat. In Fig. 13, we compare the TS values obtained from the profile log-likelihood ratio in Eq. (A14) with the one obtained from the euclideanized signals, for varying degrees of exposure and magnitude of the covariance matrix.

Appendix B: Validation of approximation methods

First, we motivate heuristically the analytical form of the fudge factor that we used in Eq. (A18). To this end, we consider the approximate relation

$$\chi_G^2 \equiv \frac{(s_1 - s_2)^2}{b + \bar{s}} \approx \chi_E^2 \equiv (x_1 - x_2)^2, \quad (\text{B1})$$

where we defined the mean signal $\bar{s} \equiv \frac{1}{2}(s_1 + s_2)$, and the Euclideanized signal

$$x_i = \frac{s_i}{\sqrt{s_i + b}} \cdot \left(1 + \frac{R \cdot s_i}{R \cdot s_i + b} \right) \quad (\text{B2})$$

As above, we set the rescaling parameter $R = 0.1$, for which we find the best performance.

The degree to which the approximation in Eq. (B1) is shown in Fig. 12, as function of the signals s_1 and s_2 . Only the region that corresponds to a signal difference of $< 5\sigma$ is shown. In this region, the approximation provides a relative agreement to within 16%. The approximation works somewhat worse if the difference between the signals becomes larger, which is however not of much relevance for the intended applications of our method.

In order to validate the Euclideanized signal method, and to estimate the expected approximation errors, we consider a large number of random models. For the purpose of illustration in this paper, we kept the models simple. They consist of $n_b = 3$ bins (we find similar results also for a much larger number of bins), with a background set to $\mathbf{B}^T = (1, 1, 1)$, a signal set to $\mathbf{S} = \theta \mathbf{R}$,

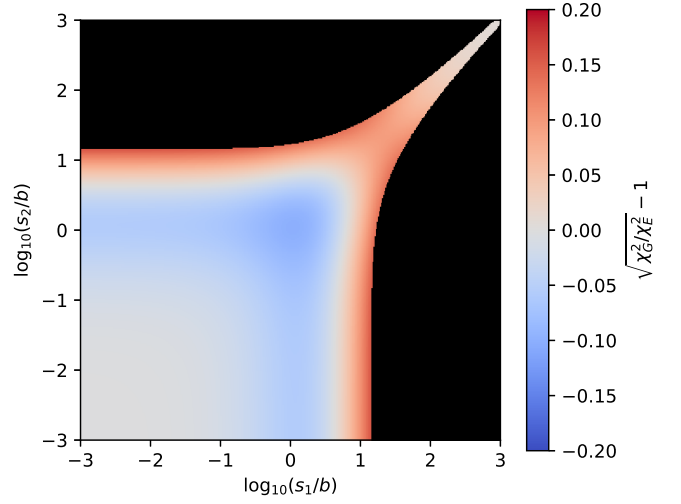


FIG. 12. Ratio between $\sqrt{\chi_G^2}$ and $\sqrt{\chi_E^2}$ in Eq. (B1), as function of s_1/b and s_2/b . The unmasked area corresponds to $\chi_G^2 < 25$, which excludes signal differences larger than $\sim 5\sigma$. Within the unmasked region, the differences between $\sqrt{\chi_G^2}$ and $\sqrt{\chi_E^2}$ are smaller than 16%.

where \mathbf{R} is a vector of random numbers in the range $[0, 1]$, and $K = k^2 L^T \cdot L$ where L is a random 3×3 matrix with entries in the range $[-1, 1]$. We assume a flat exposure given by E . We consider three benchmark scenarios. First, a *signal limited* case, with $E = 10^{-2}$, $k = 0$, $\theta = 10^{3.5}$. Second, a *systematics limited* case, with $E = 10^6$, $k = 1$, $\theta = 1$. Third, a *background limited* case that is still close to the Poissonian regime, with $E = 10^2$, $k = 0$, $\theta = 1$.

In Fig. 13 we compare the TS-value derived via the profile log-likelihood, Eq. (11), with the TS-value derived from the Euclideanized signal method, Eq. (16). We find that the deviations are largest in the signal-limited case, and up to $\pm 20\%$ on \sqrt{TS} . In the systematics limited regime, the deviations are (as expected) much smaller. Interestingly, in the background limited case, we find for the given benchmark point that there is a $\sim 10\%$ bias towards smaller TS-values. This bias disappears if we either increase the exposure (and hence the problem becomes more Gaussian), or if we decrease the exposure and the problem becomes signal dominated. We conclude that the Euclideanized signal method provides fast estimates for \sqrt{TS} that are correct to within 20%.

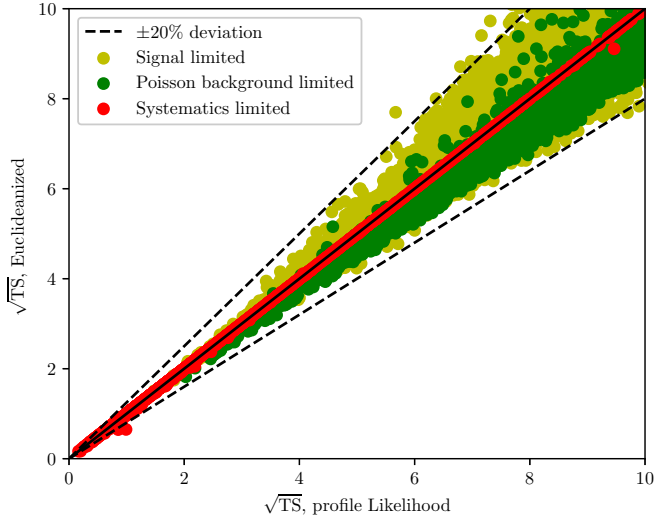


FIG. 13. Comparison between exact \sqrt{TS} value derived from the log profile-likelihood, and the approximate \sqrt{TS} value derived from the Euclideanized signal method. The different colors correspond to the signal, the systematics and the (Poisson) background limited regimes (see text for details). As indicated by the dashed lines, the deviations are not larger than 20% for all random models.